Hindawi
Journal of Chemistry
Volume 2020, Article ID 9187960, 12 pages
https://doi.org/10.1155/2020/9187960

Research Article

Coconut Shell Activated Carbon/$CoFe_2O_4$ Composite for the Removal of Rhodamine B from Aqueous Solution

Le Phuong Hoang,[1] Huu Tap Van ,[2] Thi Thuy Hang Nguyen,[1] Van Quang Nguyen,[3] and Phan Quang Thang[4]

[1]*Faculty of Civil and Environmental Engineering, Thai Nguyen University of Technology (TNUT), Tich Luong Ward, Thai Nguyen City, Vietnam*
[2]*Faculty of Natural Resources and Environment, TNU-University of Sciences (TNUS), Tan Thinh Ward, Thai Nguyen City, Vietnam*
[3]*The Center for Technology Incubator and Startup Support, Thai Nguyen University of Agriculture and Forestry, Quyet Thang Ward, Thai Nguyen City, Vietnam*
[4]*Institute of Environmental Technology (IET), Vietnam Academy of Science and Technology (VAST), 18 Hoang Quoc Viet Street, Nghia Do, Cau Giay, Hanoi, Vietnam*

Correspondence should be addressed to Huu Tap Van; tapvh@tnus.edu.vn

Received 20 July 2020; Revised 8 October 2020; Accepted 9 October 2020; Published 28 October 2020

Academic Editor: Woojin Lee

Copyright © 2020 Le Phuong Hoang et al. This is an open access article distributed under the Creative Commons Attribution License, which permits unrestricted use, distribution, and reproduction in any medium, provided the original work is properly cited.

Coconut shell activated carbon loaded with cobalt ferrite ($CoFe_2O_4$) composites (CAC/$CoFe_2O_4$) was synthesized via the single-step refluxing router method to manufacture adsorbents. The adsorbents were then applied to remove Rhodamine B (RhB) from aqueous environments via adsorption. The properties of coconut shell activated carbon (CAC) and CAC/$CoFe_2O_4$ were investigated through the usage of electron microscopic methods (SEM: Scanning Electron Microscopy, EDS: Energy Dispersive X-ray), powder X-ray diffraction (XRD), and Fourier transform infrared spectroscopy (FTIR). A series of batch experiments were implemented to evaluate the influences of various experimental parameters (initial pH, RhB concentration, contact time, and dosage of CAC/$CoFe_2O_4$) on the adsorption process. It was found that $CoFe_2O_4$ was successfully attached to activated carbon particles and had the suitable adsorption capacity for RhB at a molar ratio of 1 : 2:200 corresponding to the Co : Fe:CAC order. The removal efficiency and adsorption of RhB were optimal at a pH level of 4. The maximum adsorption capacity was 94.08 mg/g at an initial concentration of 350 mg/L and adsorbent dosage of 0.05 g/25 mL. Freundlich and Langmuir's models fitted well with the results obtained from the experimental data. The pseudo-second-order model also suited the most for RhB adsorption with the most remarkable correlation coefficient ($R^2 = 0.934$). The adsorption process was controlled by a chemisorption mechanism through electrostatic attraction, hydrogen bonding interactions, and π-π interactions.

1. Introduction

The dye pollution has always been a dramatic environmental issue lingering in developed and developing countries. Many dyes are highly toxic that not only affect the aquatic environment but also harm human health [1]. Rhodamine B dye (RhB) is a cationic xanthene dye that has been used for many industrial purposes. It presents strong fluorescent properties and high solubility in water. It is, thus, widely used in textile, paper making, painting, and lather production [2, 3]. RhB is an eye, skin, and respiratory tract irritant. Furthermore, it can cause carcinogenic, neurotoxicity, and chronic poisoning when it exists in drinking water and enters the human body [4]. Therefore, it is essential to discard RhB from drain water before discharging into nature.

A variety of technologies have been used to remove RhB from wastewater, including ion exchange, biological degradation, chemical oxidation, coagulation and flocculation, adsorption, membrane filtration, and electrochemical and reverse osmosis [5, 6]. Emerging from these methods, adsorption proves to be one of the low-cost effective techniques to remove RhB [2]. Several materials have been applied as

adsorbents to eliminate RhB from aqueous solutions such as by-agricultural products [5], activated carbon and biochar [7, 8], polymers [9], and nanomaterials [2, 6, 10]. Among all adsorbent materials, activated carbon (AC) appears to be drastically efficient in adsorbing dyes with a high adsorption capacity [11]. However, it is difficult to separate AC powder after the adsorption process. Thus, some studies focused on the application of magnetically separable AC composites as a low-cost adsorbent with a high solid-liquid separation ability and significant effectiveness. Bagheri et al. [12] made an investigation to make Fe_3O_4 magnetite nanoparticles and afterward to load them on active carbon to enhance the efficiency in the elimination of methylene blue, Sunset yellow, and Eosin b. Fayazi et al. [13] also did a study to make activated carbon/γ-Fe_2O_3 a nanocomposite Alizarin red S adsorption from aqueous samples with the maximum adsorption capacity reaching 108.69 mg/g. Feiqiang et al. [14] synthesized magnetic-activated carbons by the modified one-step method for removing malachite green from solutions. Spinel $CoFe_2O_4$ is a magnetic material with drastic anisotropy and high coerciveness at room temperature. Moreover, $CoFe_2O_4$ has excellent physical and chemical stability [15] for dye adsorption. Therefore, combining AC and $CoFe_2O_4$ nanoparticles also has been studied to make efficient adsorbent with highly magnetic separating ability. Ai et al. [16] successfully manufactured activated carbon/$CoFe_2O_4$ composite (AC/CFO) by the simple one-step refluxing route for adsorbing malachite green. Reports of the study showed that AC/CFO could be utilized as a promising and effective adsorbent to adsorb malachite green with the adsorption capacity of 89.29 mg/g. Liang et al. [15] did a study to make $CoFe_2O_4$/activated carbon ($CoFe_2O_4$/AC) through a one-step low-temperature refluxing route to adsorb gentian violet. This material presented a remarkable adsorption capacity of gentian violet with 184.2 mg/g at 303°K. Qiu et al. [17] made an investigation to make $CoFe_2O_4$/activated carbon composites by a simplified hydrothermal technique for removing Cr(VI) from wastewater. The results specified that the Cr(VI) adsorption process using $CoFe_2O_4$/activated carbon was more powerful than the pristine AC. According to the current knowledge, the effect of molar ratios of Co : Fe:AC on making $CoFe_2O_4$/AC for dye adsorption is still unclear though there were a few reports of systematic in-depth studies examining the adsorption of RhB onto $CoFe_2O_4$/AC composites.

In this study, activated carbon was produced from coconut shell (CAC), and activated carbon/$CoFe_2O_4$ was prepared through a single-step refluxing router with various molar ratios of Co : Fe:CAC. The analyses of the physicochemical properties of the adsorbent material were apprehended by SEM, EDX, XRD, and FTIR. The adsorption process was investigated with parameters including molar ratios of Co : Fe:CAC, solution pH, contact time, initial Rhodamine B (RhB) concentration, and adsorbent dosage. The evaluations of isotherm, adsorption kinetics, and mechanism of RhB adsorption onto activated carbon/$CoFe_2O_4$ were also investigated in batch experiments.

2. Materials and Methods

2.1. Material. The chemicals that were applied during experiments included ferric nitrate nonahydrate ($Fe(NO_3)_3.9H_2O$, 99%), cobalt nitrate hexahydrate ($Co(NO_3)_2.6H_2O$, 99%), sodium hydroxide (NaOH, >99%), and Rhodamine B ($C_{28}H_{31}N_2O_3Cl$, >90%) were obtained by Merck. The stock Rhodamine B (RhB) solution at a concentration of 500 mg/L was produced by dissolving 0.5 g RhB in 1000 mL of distilled water. All experimental solutions were achieved by diluting the stock solution with distilled water.

2.2. Preparation of Coconut Activated Carbon/$CoFe_2O_4$ (CAC/$CoFe_2O_4$). The coconut shell was collected from Ben Tre province, Vietnam. At first, the coconut shell was rinsed several times with tap water and afterward with distilled water to remove surface dust before being dried at 105°C to obtain a constant weight of dry matters. Then, the dried coconut shell was crushed until a particle diameter ranges from 10 to 100 mm. Next, the coconut activated carbon (CAC) was processed by heating under slow pyrolysis at 700°C for 3 h in a Nabertherm furnace (model L3/11/B170, Germany) under water stream in nitrogen at a flow rate 100 mL/min. Afterward, the furnace was cooled down to the ambient temperature and the products were ground until the size of each particle was less than 0.5 mm. CAC was, then, cleansed and dried in an oven at 105°C for 2 h.

The CAC/$CoFe_2O_4$ composites were synthesized by a single-step refluxing router [16]. In this synthesis process, 3.4 g NaOH was diluted in 150 mL distilled water before adding a certain proportion of CAC and stirring for 30 min at room temperature to gain activated carbon suspension. The suspension was maintained at the boiling state by 100°C heating. 50 mL solution containing 5.4944 g $Fe(NO_3)_3{\cdot}9H_2O$ and 1.9790 g $Co(NO_3)_2{\cdot}6H_2O$ was poured quickly into the boiling suspension. The composition of CAC was calibrated according to molar ratios of Co : Fe: CAC at 1 : 2:300, 1 : 2:250, 1 : 2:200, 1 : 2:150, and 1 : 2:100. The mixture solution was circulated at 100°C for 2 h. Subsequently, CAC/$CoFe_2O_4$ composite products were separated by a magnet before being dried at 80°C within 12 h. The obtained materials were labeled as CAC/$CoFe_2O_4$300, CAC/$CoFe_2O_4$250, CAC/$CoFe_2O_4$200, CAC/$CoFe_2O_4$150, and CAC/$CoFe_2O_4$100 and stored for further uses.

2.3. Characterization of CAC/$CoFe_2O_4$. The Brunauer–Emmett–Teller (BET) surface area and the pore structure of CAC and CAC/$CoFe_2O_4$ were analyzed by Micromeritics SSA-4300 surface analyzer. The surface morphology of prepared samples was determined by energy-dispersive X-ray spectroscopy (Hitachi S-4800) with EDS and SEM systems. The crystalline structures of CAC, CAC/$CoFe_2O_4$, and RhB–CoFe/CAC were determined by the X-ray diffraction technique using XRD-D8 ADVANCE with Cu Ka radiation ($\lambda = 1.5417$ Å). The 2θ angle scanned from 10° to 70° at a scanning speed of 3°/min. The

identification of functional groups of CAC/$CoFe_2O_4$ before and after adsorbing Rhodamine B was clarified by Fourier transform infrared spectroscopy (FTIR-6300) in a range of 500–4000 cm^{-1}. The magnetic property of CAC/$CoFe_2O_4$ was measured at room temperature using a vibrating sample magnetometer (VSM LakeShore 7404). The pH value at zero charges (pH_{PZC}) was obtained by the Mular-Robert titration method [18]. A known amount of CAC/$CoFe_2O_4$ (1 g) was put into 100 mL of 0.1 M KCl solution with pH adjustment in the range from 2 to 12 done by the addition of 0.1 M NaOH or 0.1 M HCl (pH_{is}). The flasks then were sealed and shaken in 24 hours before recording the final solution pH (pH_{fs}). The ΔpH values ($\Delta pH = pH_{is} - pH_{fs}$) were orchestrated against pH_{is}. The pH_{PZC} represents the intersection point of the curve and ΔpH.

2.4. Adsorption Procedure. Adsorption experiments of RhB onto CAC/$CoFe_2O_4$ were conducted using a batch equilibrium technique. All experiments were performed in triplicate. A certain amount of CAC/$CoFe_2O_4$ was placed in 50 mL Erlenmeyer flasks that contained 25 mL of RhB at various concentrations. The flasks were secured with paraffin and afterward agitated at 120 rpm by the PH-4A shaker machine (China) at ambient temperature. The management of solution pH was carried out by using HCl 0.1 M and NaOH 0.1 M. After the adsorption process was finished, adsorbents were filtered from the dye sample using 0.11 μm filter paper. The content of RhB in the suspended solution was determined at 554 nm using a UV-Vis spectroscopic method [19]. The RhB adsorption capacity of CAC/$CoFe_2O_4$ calculations at time t (denoted as q_t, division: mg/g) and equilibrium (denoted as q_e, division mg/g) was identified by equations (1) and (2), respectively:

$$q_t = \frac{(C_o - C_t)V}{m}, \quad (1)$$

$$q_e = \frac{(C_o - C_e)V}{m}, \quad (2)$$

where C_o (mg/L), C_t (mg/L), and C_e (mg/L) are RhB concentrations in the solution at the beginning time, random time t, and equilibrium, respectively. V (L) is the volume of the RhB solution and m (g) is the mass of the CAC/$CoFe_2O_4$.

2.5. Data Analysis. The obtained data from experimenting was processed for analysis by Origin software 8.1. The error bars in all figures appear for the standard deviation of a triplicate test.

3. Results and Discussion

3.1. Optimizing the Ratio of CAC and $CoFe_2O_4$ to Produce CAC/$CoFe_2O_4$ on Rhodamine B Adsorption. The experiments were carried out in order to apprehend the evaluation of the adsorption capacity of CAC, $CoFe_2O_4$, and CAC/$CoFe_2O_4$ at various molar ratios of Co : Fe : CAC (1 : 2 : 300; 1 : 2:250; 1 : 2 : 200; 1 : 2 : 150, and 1 : 2 : 100). Other parameters were set with an adsorbent dose of 0.05 g/25 mL, initial RhB concentration of 50 mg/L, and adsorption time of 60 min at room temperature.

Figure 1 indicates that the adsorption capacity of CAC/$CoFe_2O_4$ for RhB was better than that of CAC and $CoFe_2O_4$. The adsorption capacity of CAC and $CoFe_2O_4$ only reached 8.15 mg/g and 9.67 mg/g, respectively, while it increased from 13.57 mg/g to 17.68 mg/g with increasing molar ratios of Co : Fe in making CAC/$CoFe_2O_4$ adsorbent (Co : Fe : CAC at 1 : 2:300; 1 : 2 : 250, and 1 : 2 : 200). This is due to the existence of $CoFe_2O_4$ nanoparticles in the micropores of CAC that can coordinate highly with the carboxyl group in molecular Rhodamine B [20]. However, the adsorption capacity of bare $CoFe_2O_4$ was also lower than of CAC/$CoFe_2O_4$ composites because of its lower specific surface area and pore volume [15, 21]. Figure 1 also shows that the adsorption capacity of CAC/$CoFe_2O_4$ for RhB decreased with the molar ratios of Co : Fe:CAC at 1 : 2:150 and 1 : 2:100. This may be a saturation of the active sites on CAC/$CoFe_2O_4$ surfaces. Thus, there were not active sites sufficient for the attachment of RhB onto CAC/$CoFe_2O_4$ [22]. According to the above result, CAC/$CoFe_2O_4$ synthesized at a molar ratio of Co : Fe:CAC that is 1 : 2:200 (CAC/$CoFe_2O_4$200) shows the highest adsorption capacity for RhB. Therefore, it was chosen for further experiments.

3.2. Characterization of Activated Carbon-$CoFe_2O_4$ Composite (CAC/$CoFe_2O_4$). The Brunauer–Emmett–Teller (BET) results disclose that CAC has a large specific surface area of 867.449 m^2/g, and the average pore volume was 0.381 cm^3/g. However, the presence of $CoFe_2O_4$ affected the characteristics of CAC/$CoFe_2O_4$ with a slight decrease of the surface area (to 759.638 m^2/g) and pore volume of CAC/$CoFe_2O_4$200 (to 0.321 cm^3/g), respectively. This can explain that the $CoFe_2O_4$ has loaded on the coconut activated carbon leading to the benefits of adsorbing other molecules [23]. Similar results were obtained in previous reports of magnetic oxide/activated carbon composites [16, 24]. The results of SEM from Figures 2(a) and 2(b) indicated that the structure of CAC was modified after being composited by $CoFe_2O_4$. Besides, the results of EDS analysis revealed that CAC is composed of 100% C (Figure 2(b)). However, Co, Fe, and O elements appeared in CAC/$CoFe_2O_4$200 with the percentages of elements for C, O, Fe, and Co that were 70.89%, 20.64%, 5.28%, and 3.18%, respectively (Figure 2(d)). This indicates that $CoFe_2O_4$ particles were successfully attached to the coconut activated carbon surface. After RhB was adsorbed onto the adsorbent (CAC/$CoFe_2O_4$200–RhB), the proportion of element for C changed to 78.42% while O, Fe, and Co elements were 16.84%, 3.25%, and 1.48%, respectively (Figure 2(f)). These results may be due to the effect of the RhB adsorption process onto CAC/$CoFe_2O_4$200.

The magnetic behavior of the CAC/$CoFe_2O_4$200 was carried out using a vibrating sample magnetometer (VSM) at room temperature (25 ± 2°C). The result is shown in Figure 3. The saturation magnetization (Ms) of CAC/

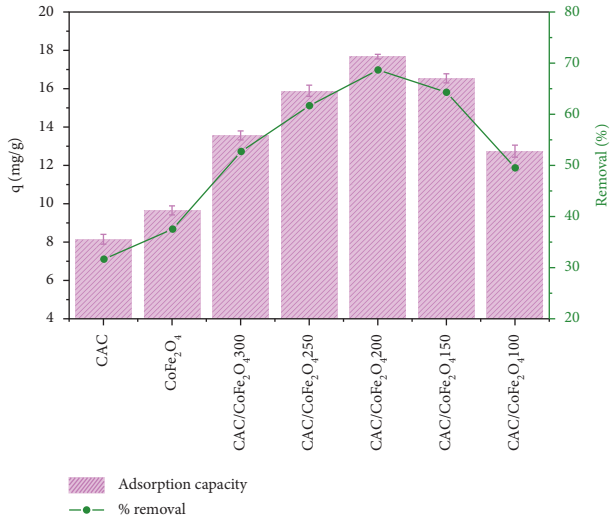

FIGURE 1: The effect of various molar ratios of Co : Fe : CAC on RhB adsorption at 50 mg/L of initial Rhodamine B, 60 min of contact time, and 0.05 g of adsorbent dosage/25 mL RhB.

$CoFe_2O_4200$ was 7.22 emu/g that was near to the values of AC/CFO material ($Ms = 7.6$ emu/g) reported by Ai et al. [16] and of $CoFe_2O_4$/AC material ($Ms = 6.93$ emu/g) reported by Qiu et al. [17]. These values indicated that CAC/$CoFe_2O_4200$ can be used as a magnetic absorbent to remove pollutants in water.

3.3. Effect of pH. The impacts caused by initial solution pH to the RhB adsorption capacity of CAC/$CoFe_2O_4200$ were investigated in the pH range of 2.0 to 10.0, CAC/$CoFe_2O_4200$ dosage of 0.05 g/25 mL, initial RhB concentration of 50 mg/L, and contact time of 60 min at room temperature ($25 \pm 2^{\circ}C$). The result is shown in Figure 4(a). In the pH level ranging from 2 to 4, the removal efficiency and adsorption capacity for RhB increased sharply from 30.26 to 60.98% and 9.14 to 18.81 mg/g, respectively, whereas the pH level of 4 to 8 made the adsorption capacity of CAC/$CoFe_2O_4200$ to RhB relatively stable. However, there were significant declines in the sorption capacity as well as the removal efficiency of RhB corresponding to the increase in pH from 9 to 10. To make an explanation for this result, we need to consider the structure of RhB dye and the zero point charge of CAC/$CoFe_2O_4200$. At solution pH lower than 3.5, RhB ions are cationic (RhB^+) and molecules are in monomeric form. When pH is higher than 3.5, the zwitterionic form of RhB ($RhB^{\pm}$) increased [8]. Moreover, pH_{PZC} of CAC/$CoFe_2O_4200$ was 8.34. At solution pH below pH_{PZC} (<8.34), the surface of CAC/$CoFe_2O_4200$ was positively charged with more H^+ ions while RhB at pH < 3.5 was also cationic. Thus, H^+ ions might compete with RhB^+ cations in solution causing low adsorption [25]. At pH above 3.5, the adsorption capacity grew sharply due to the surface of RhB that was changed to zwitterionic form causing the attractive electrostatic interactions between $RhB^{\pm}$ ions and the surface of CAC/$CoFe_2O_4200$ [6]. However, at solution pH ≥ 9, the deprotonation of RhB dye increased and the surface of CAC/$CoFe_2O_4200$ was negatively charged leading to the decrease in adsorption rate [26]. Similar results were reported in some studies [10, 25].

3.4. Effect of Contact Time. Contact times also cause influences on the RhB adsorption capacity of CAC/$CoFe_2O_4200$. The experiments were conducted at a solution pH of 4.0, initial RhB concentration of 50 mg/L, adsorbent dose of 0.05 g/25 mL, and contact time set variously from 5 to 210 min. Figure 5 indicates that the adsorption capacity and removal efficiency of RhB grew rapidly from 8.07 to 18.09 mg/g and from 29.65 to 66.46%, respectively, for the first 60 min of contact time. While extending the contact time, the adsorption of RhB slowed down and reached equilibrium at 150 min with the maximum adsorption capacity and removal efficiency that were 23.14 mg/g and 84.98%, respectively. This could be due to the fact that at the initial stage of the adsorption process, the surface of CAC/$CoFe_2O_4200$ had a large number of active sites available for RhB attachment. After that, because of adsorption of RhB molecules on the CAC/$CoFe_2O_4200$ surface leading to saturation of adsorption sites, the adsorption reduced and became stable at equilibrium point [10]. Some other studies also reported a similar tendency [27, 28].

3.5. Effect of Absorbent Dose. The experiment studying the effects of applied CAC/$CoFe_2O_4200$ doses on RhB adsorption was arranged at different dosages ranging from 25 to 200 mg/25 mL, initial RhB concentration of 50 mg/L, solution pH of 4, and contact time of 150 min. The results are given in Figure 6. It was observed that with the CAC/$CoFe_2O_4200$ dosage increasing from 25 to 100 mg/25 mL, the RhB removal efficiency increased significantly from 62.96% to 92.34%. The result may be explained following an increase of active sites corresponding to the increased CAC/$CoFe_2O_4200$ dosage [1]. However, the percentage of adsorption did not increase and became stable as the adsorbent dose further increased from 100 to 200 mg/25 mL, whereas the RhB adsorption capacity reduced from 34.29 to 6.26 mg/g corresponding to CAC/$CoFe_2O_4200$ dose rising from 25 to 200 mg/25 mL. All experiments were investigated at constant initial RhB concentrations and volumes. Therefore, the active sites on CAC/$CoFe_2O_4200$ surface may be saturated when the adsorbent dose increased causing the decrease in adsorption capacity [29]. The above results showed that the applied adsorbent dosage plays a vital role in the adsorption process, which was also found in other studies [7, 28].

3.6. Effect of Initial Rhodamine B Concentration. As a factor that considerably affects the adsorption capacity, the initial RhB concentration and its effects require clarification and evaluation. The experiment examining the influence of variations of the initial RhB concentration from 20 to 400 mg/L on its adsorption onto CAC/$CoFe_2O_4200$ was conducted with an absorbent dosage of 50 mg/25 mL, solution pH of 4, and the contact time of 150 min. It was discovered that the adsorption capacity of RhB onto CAC/$CoFe_2O_4200$ increased and reached the maximum at 94.08 mg/g as the

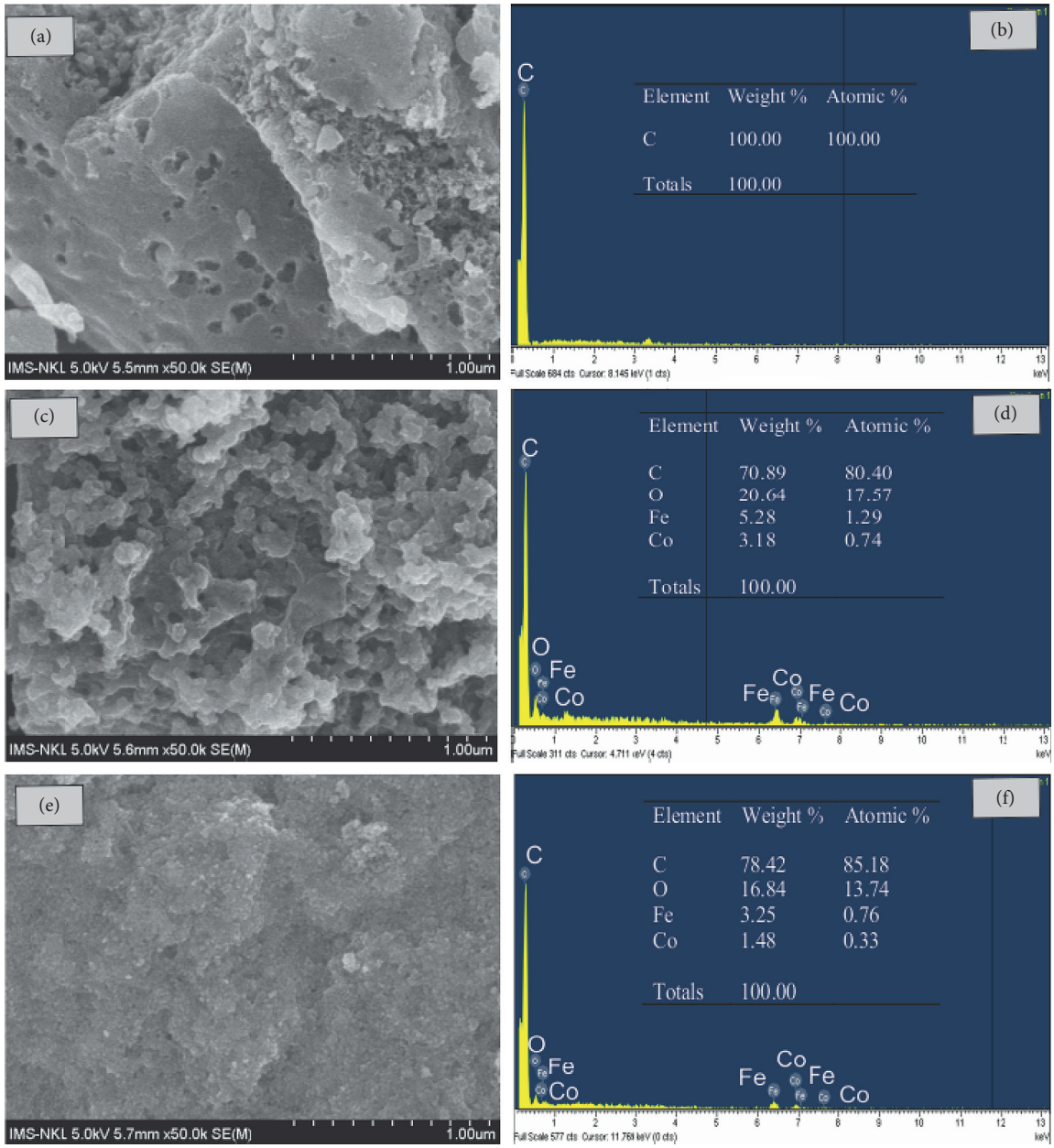

Figure 2: SEM image and EDS spectra of (a, b) coconut activated carbon (CAC), (c, d) CAC/$CoFe_2O_4$200, and (e, f) CAC/$CoFe_2O_4$200 after adsorption Rhodamine B (CAC/$CoFe_2O_4$200–RhB).

initial RhB concentration raised to 350 mg/L (Figure 7). However, the adsorption capacity did not increase and became stable at the initial RhB concentration of more than 350 mg/L. Otherwise, the removal efficiency of RhB decreased from 93.29% to 45.56% corresponding to the initial RhB concentration growing from 20 to 400 mg/L. This phenomenon can be due to the fact that at a higher concentration, the driving force of the concentration gradient rises leading to the increasing adsorption capacity [30]. However, with the fixed amount of adsorbent dosage, the adsorption sites were limited. Thus, at a higher RhB concentration, the ratio of activating sites and RhB molecules was low causing the decrease in RhB removal [10]. Some previous studies such as the study of RhB adsorption onto kaolinite [28] or MgO supported Fe–Co–Mn nanoparticles [2] also had the same tendency.

3.7. Isotherm Modeling. The distribution of Rhodamine B molecules between the liquid state and the solid state can be provided by the isotherm parameters. Langmuir, Freundlich, and Temkin isotherm models were utilized as analyzers for the gathered experimental data. According to the Langmuir model, it is assumed that the energy of all adsorption sites is equivalent, the sorption surface is homogeneous, and molecule adsorption processes do not interact with each other [31]. Meanwhile, the Freundlich model

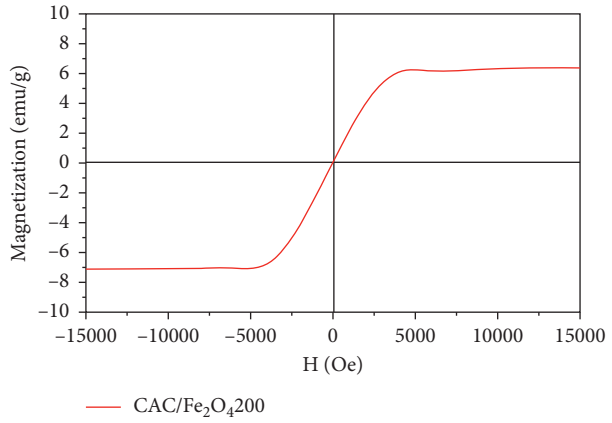

Figure 3: Magnetic hysteresis curves of CAC/$CoFe_2O_4$200.

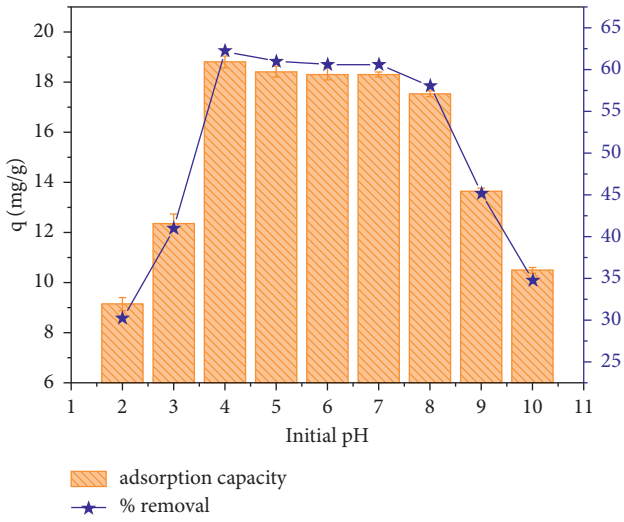

(a)

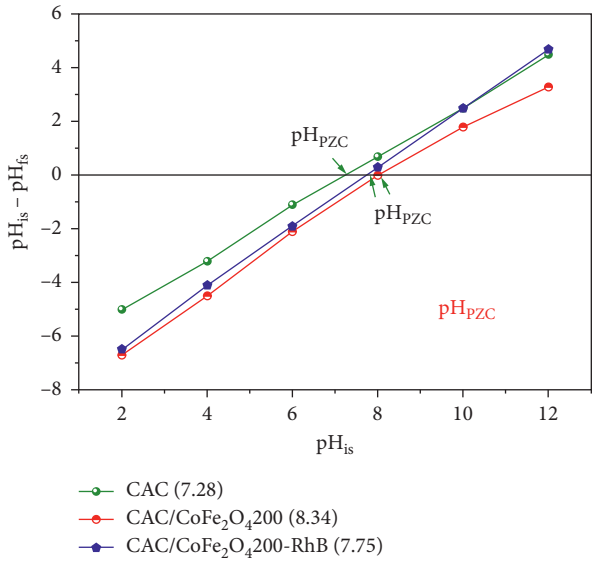

(b)

Figure 4: Effects of different pH levels on RhB adsorption by CAC/$CoFe_2O_4$200 at 50 mg/L of initial RhB, 60 min of contact time, 0.05 g CAC/$CoFe_2O_4$200/25 mL RhB of adsorbent dosage (a), and pH_{PZC} of CAC/$CoFe_2O_4$200 (b).

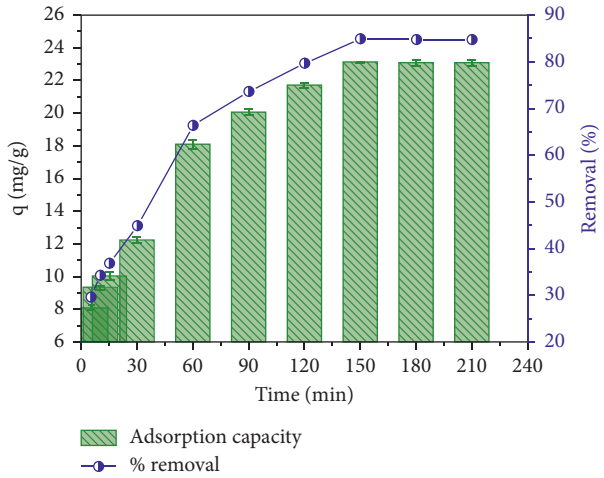

Figure 5: Effects of contact times on RhB adsorption by CAC/$CoFe_2O_4$200 at 50 mg/L initial RhB concentration, adsorbent dosage of 0.05 g CAC/$CoFe_2O_4$200/25 mL RhB, and initial pH of 4.

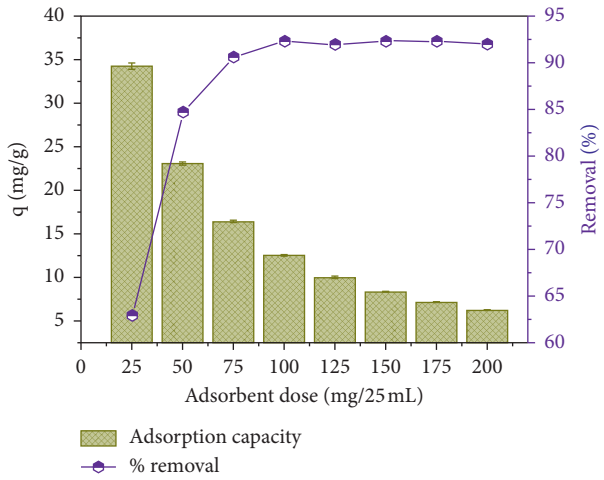

Figure 6: Effect of adsorbent dosage on RhB adsorption by CAC/$CoFe_2O_4$200 at 50 mg/L of initial RhB, 150 min of contact time, and initial pH of 4.

explains the multilayer adsorption on heterogeneous surfaces and the difference in the energy of all adsorption sites [6]. On the other hand, Temkin isotherm supposes that the heat of adsorption reduces linearly and binding energies were distributed uniformly [28]. The equations of Langmuir, Freundlich, and Temkin models are described as shown in (3) [31], (4) [6], and (5) [28], respectively:

$$q_e = \frac{q_m K_L C_e}{1 + K_L C_e}, \tag{3}$$

$$q_e = K_f C_e^{(1/n)}, \tag{4}$$

$$q_e = \frac{RT}{b} \ln\left(A_T C_e\right), \tag{5}$$

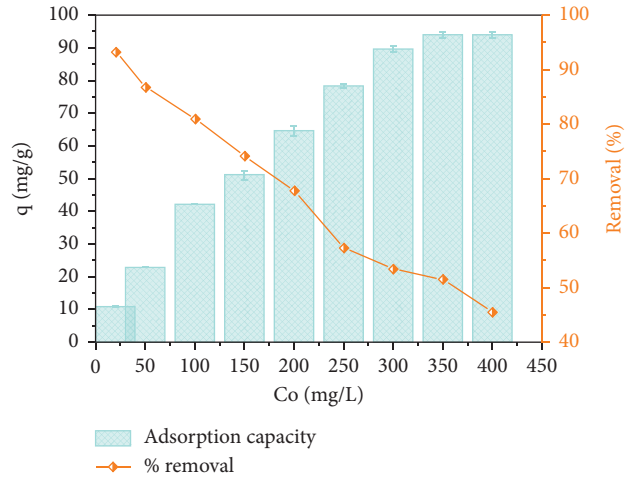

Figure 7: Effect of initial RhB concentrations on the adsorption process by CAC/$CoFe_2O_4$200 at initial pH of 4, 150 min of contact time, and adsorbent dosage of 0.05 g/25 mL.

where C_e and q_e are the RhB concentration and the adsorption capacity (mg/g) at equilibrium (mg/L), respectively, q_m is the Langmuir adsorption capacity (mg/g), K_L is the Langmuir constant (L/mg), K_f is the Freundlich coefficient (mg/g), n is the adsorption intensity, A_T is the Temkin isotherm equilibrium binding constant (L/g), b is the Temkin isotherm constant (J/mol), R is the universal gas constant (8.314 J/mol/K), and T is the temperature at 298 K.

Figure 8 and Table 1 show the results of Langmuir, Freundlich, and Temkin isotherm models for the adsorption of RhB onto CAC/$CoFe_2O_4$200. According to the calculated data, the correlation coefficient for the Freundlich isotherm model (0.985) was higher than the values obtained for Langmuir (0.978) and Temkin (0.957) isotherm. This expressed that the RhB adsorption onto CAC/$CoFe_2O_4$200 isotherm fitted well with the Freundlich model. This indicated that the mechanism of RhB adsorption was multilayer and the surface of the adsorbent was heterogeneous [10]. In addition, the *1/n* value given by the Freundlich equation was $0.377 < 1$, which confirmed the favorability of RhB adsorption onto CAC/$CoFe_2O_4$200 [6, 32]. However, for the Langmuir model, R^2 value was 0.978 and the q_m value was approximately 107.48 mg/g corresponding to q_{mexp} (94.08 mg/g). This evidenced that the monolayer adsorption also had a vital part in the reception of RhB onto CAC/$CoFe_2O_4$200 [33]. The Langmuir maximum adsorption capacity of RhB onto CAC/$CoFe_2O_4$200 compared with other adsorbents was also reported in the references (Table 2). It can be seen that the adsorption capacity of CAC/$CoFe_2O_4$200 for RhB is relatively higher than some adsorbents (Jute stick powder, Fe_3O_4/Al pillared bentonite, cobweb-mediated AgNPs, kaolinite, duolite C-20 resin, and surfactant-modified coir pith) but lower than that of Gg-Cl-P(AA-Co-AAm)/Fe_3O_4 nanocomposites, $CoFe_2O_4$@vacancy@mSiO_2, and Zn/CoZIF-derived carbon.

3.8. Adsorption Kinetics. The adsorption kinetics of RhB onto CAC/$CoFe_2O_4$200 were clarified through the

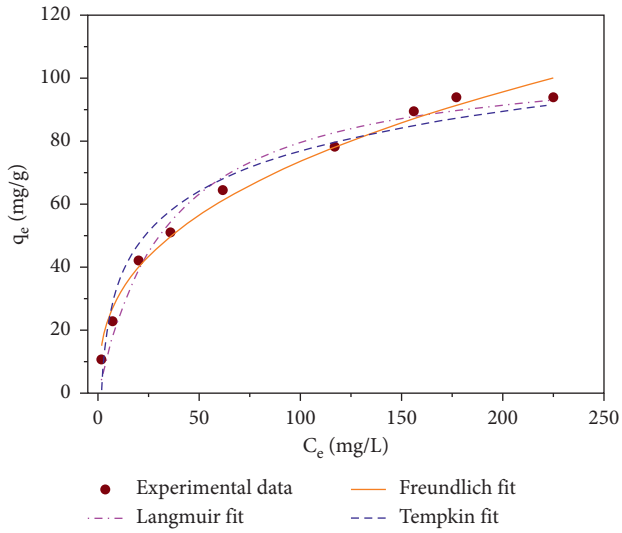

Figure 8: Adsorption isothermal equilibrium tendency of RhB onto CAC/$CoFe_2O_4$200 at the contact time of 150 min, the absorbent dose of 0.05 mg/25 mL, and the initial pH of 4.

Table 1: The adsorption isothermal parameters of RhB onto CAC/$CoFe_2O_4$200.

Langmuir model			Freundlich model			Temkin model			q_{mexp}(mg/g)
q_m(mg/g)	K_L	R^2	K_F	1/n	R^2	A_T	b	R^2	
107.48	0.028	0.978	12.975	0.377	0.984	0.686	136.425	0.957	94.08

contribution of the pseudo-first-order (6) and pseudo-second-order models (7) [9].

$$\ln(q_e - q_t) = \ln q_e - k_1 t, \tag{6}$$

$$\frac{t}{q_t} = \frac{1}{k_2 q_e^2} + \frac{1}{q_e} t, \tag{7}$$

where q_t (mg/g) and q_e (mg/g) are the adsorption capacity at time t and at equilibrium, respectively, k_1 (min^{-1}) is the first-order rate constant, and k_2 (g/mg·min) is the second-order rate constant.

The results of linear models fitting the experimental data with pseudo-first-order and pseudo-second-order models are expressed in Figure 9, and the kinetic parameters are shown in Table 3. The value of correlation coefficient (R^2) of the RhB adsorption onto CAC/$CoFe_2O_4$200 achieved via the pseudo-second-order equation (7) was 0.934, while the correlation coefficient value of the pseudo-first-order was $R^2 = 0.874$. Besides, the adsorption capacity calculated ($q_{e\,cal}$) from pseudo-second-order was 25.26 mg/g, which was relatively fitting with the experimental result ($q_{e\,exp}$ = 23.14 mg/g). These indicated that the adsorption of RhB onto CAC/$CoFe_2O_4$200 followed the pseudo-second-order kinetic model and the adsorption process inclined more toward chemisorption [6]. The same result was also reported in the RhB adsorption onto cobalt nanoparticles-embedded magnetic ordered mesoporous carbon (Co/OMC) [39], $CoFe_2O_4$@vacancy@mSiO_2 [10], and Zn/Co ZIF-derived carbon [34].

3.9. Proposed Adsorption Mechanisms. The RhB adsorption process and functional groups available on the surface of CAC/$CoFe_2O_4$200 share a firm association. The surface characteristics of adsorbents are affected by the type and quantity of functional groups that are identified by FTIR (Figure 10). The FTIR spectral results show the difference of the functional groups presenting in CAC, CAC/$CoFe_2O_4$200, and CAC/$CoFe_2O_4$200–RhB. A peak at approximately 3660 cm^{-1} proposed the stretching of the O–H group [40, 41] in all CAC, CAC/$CoFe_2O_4$200, and CAC/$CoFe_2O_4$200–RhB. Two broad peaks at around 2981 cm^{-1} and 2900 cm^{-1} are involved in the C-H stretching in alkane groups [42]. A small peak at 2319 cm^{-1} pointed out the stretching vibration of C≡C [30]. The peaks at 1392 cm^{-1} and 1479 cm^{-1} corresponded to the symmetrical C-H vibration [30]. The strong peaks in the range from 1050 cm^{-1} to 1288 cm^{-1} also marked the C-O stretching vibration [15, 42]. The peaks observed in the range from 698 cm^{-1} to 894 cm^{-1} were about the C-H group [42]. However, the peaks at around 1741 cm^{-1} and 1604 cm^{-1} corresponding to the C=O vibration and the C=C stretching vibration of the aromatic ring, respectively [40], appeared in CAC but disappeared in CAC/$CoFe_2O_4$200 and CAC/$CoFe_2O_4$200–RhB. Besides, in CAC/$CoFe_2O_4$200 and CAC/$CoFe_2O_4$200–RhB, the peaks at 1392 cm^{-1} in the range from 1050 cm^{-1} to 1288 cm^{-1} and from 698 cm^{-1} to 894 cm^{-1} were weaker than those in CAC. In addition, in the FTIR spectra of CAC/$CoFe_2O_4$200 and CAC/$CoFe_2O_4$200–RhB, the peaks appeared at 1977 cm^{-1} and 1934 cm^{-1} compared to the FTIR spectra of CAC which represented C=O groups [43]. This was due to the effect of

Table 2: Comparison of RhB adsorption capacity on CAC/$CoFe_2O_4$200 with other adsorbents.

Adsorbent	Equilibrium RhB concentration range (mg/L)	Isotherms	Langmuir maximum adsorption capacity (mg/g)	References
Gg-Cl-P(AA-Co-AAm)/Fe_3O_4 nanocomposites	0–200	Langmuir	529.10	[1]
$CoFe_2O_4$@vacancy@mSiO_2	—	Freundlich and Langmuir	154.08	[10]
Zn/CoZIF-derived carbon	0–200	Langmuir and Freundlich	116.2	[34]
CAC/$CoFe_2O_4$200	0–250	Freundlich and Langmuir	107.48	This study
Jute stick powder	0–200	Langmuir and Freundlich	87.7	[35]
Fe_3O_4/Al pillared bentonite	0–350	Langmuir	62.15	[36]
Cobweb-mediated AgNPs	0–35	Langmuir	59.85	[6]
Kaolinite	0–30	Langmuir	46.08	[28]
Duolite C-20 resin	0–1.6	Langmuir and Freundlich	28.57	[37]
Surfactant-modified coir pith	0–50	Langmuir and Freundlich	14.90	[38]

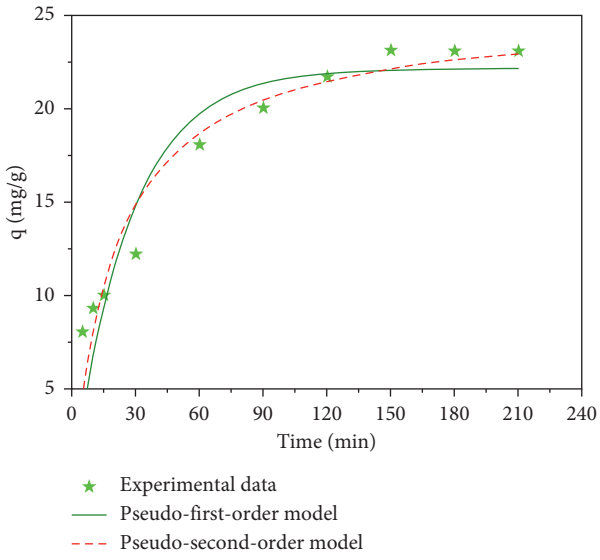

Figure 9: Kinetic models of RhB adsorption onto CAC/$CoFe_2O_4$200 with the initial RhB concentration of 50 mg/L, adsorbent dosage of 0.05 mg/25 mL, and initial pH of 4.

Table 3: Calculated kinetic parameters of models for RhB adsorption onto CAC/$CoFe_2O_4$200.

Pseudo-first-order			Pseudo-second-order			
$q_{e,cal}$ (mg/g)	k_1	R^2	$q_{e,cal}$ (mg/g)	k_2	R^2	$q_{e,exp}$ (mg/g)
22.17	0.037	0.874	25.26	0.0019	0.934	23.14

$CoFe_2O_4$ particles presenting in the CAC/$CoFe_2O_4$200's surface.

According to the functional groups that are on the surface of CAC, CAC/$CoFe_2O_4$200, and CAC/$CoFe_2O_4$200–RhB, the carboxylic and hydroxyl groups on the active sites might be accountable for the adsorption of RhB molecules that shared positive charge. It might be due to the properties of RhB as a cationic dye with a carboxylic group [44]. The calculated results of isotherm models and adsorption kinetics indicated that monolayer, multilayer, and chemisorption were dominated for RhB adsorption onto CAC/$CoFe_2O_4$200. Therefore, the negatively charged surface and positive charged + $NH–CH_3$RhB molecules might be formed owing to the electrostatic attraction, hydrogen bonding interaction, and π-π interaction [45]. Additionally, the new peaks at 35.61° and 61.78° (Figure 11) appeared in XRD pattern results of CAC/$CoFe_2O_4$200 and CAC/$CoFe_2O_4$200–RhB which revealed the appearance of the cubic spinel phase structure of $CoFe_2O_4$ [17, 46]. These results further confirmed that the $CoFe_2O_4$ cubic spinel existed in CAC/$CoFe_2O_4$200 composites

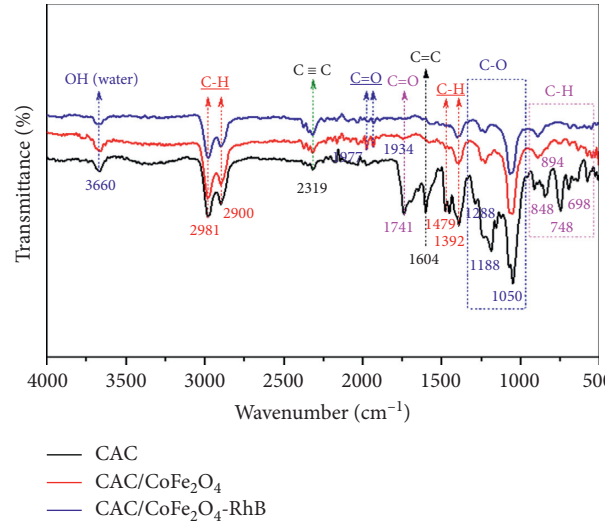

Figure 10: FTIR graph of CAC, CAC/$CoFe_2O_4$200, and CAC/$CoFe_2O_4$200–RhB.

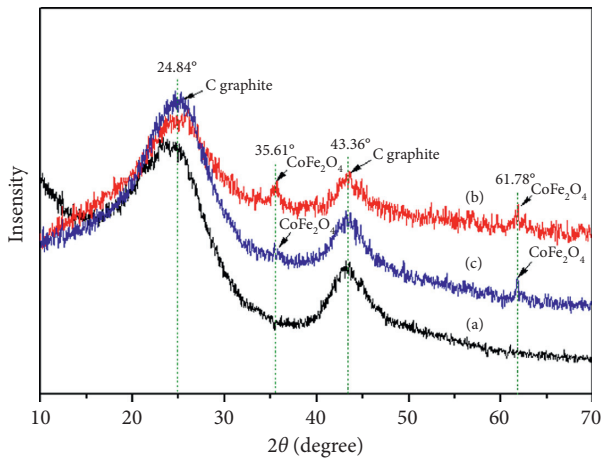

Figure 11: XRD graphs of (a) CAC, (b) CAC/$CoFe_2O_4$200, and (c) CAC/$CoFe_2O_4$200–RhB.

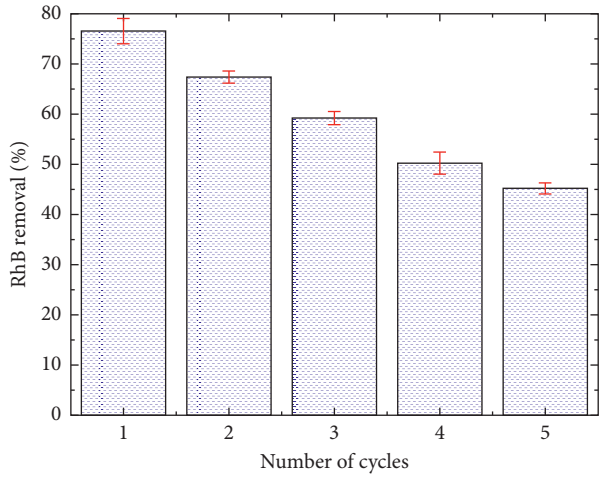

Figure 12: RhB adsorption efficiency of CAC/$CoFe_2O_4$200 after adsorption/desorption cycles.

corresponding to the obtained numbers of SEM and EDS spectra (Figures 2(c)–2(f)). The RhB adsorption capacity of CAC/$CoFe_2O_4$200 was higher than the capacity of CAC due to the successful attachment of $CoFe_2O_4$ on CAC. The results suggested that the $CoFe_2O_4$ loaded onto CAC played a significant role in RhB adsorption by CAC/$CoFe_2O_4$200.

Moreover, pH_{PZC} also contributed to the determination of adsorption mechanisms of RhB onto CAC/$CoFe_2O_4$200. In this study, the solution $pH < pH_{PZC}$ indicated that there were negative charged functional groups appearing on the surface of CAC/$CoFe_2O_4$200. The pH_{PZC} of CAC/$CoFe_2O_4$200–RhB being less than that of CAC/$CoFe_2O_4$200 also demonstrated that RhB was adsorbed by the chemisorption mechanism. The presence of $CoFe_2O_4$ on the adsorbent proved its importance to increase the pH_{PZC} of CAC/$CoFe_2O_4$200. These above-mentioned results asserted that RhB adsorption onto the surface of CAC/$CoFe_2O_4$200 was enhanced by various types of interactions. Based on the above results and comparisons of adsorption properties of CAC/$CoFe_2O_4$200 with homogeneous adsorbents, it might be concluded that CAC/$CoFe_2O_4$200 is potential for dye removal from wastewater.

3.10. Regeneration of Adsorbent. The reuse of adsorbent is the requirement to minimize the cost of adsorption processes. Therefore, CAC/$CoFe_2O_4$200 should be regenerated after RhB adsorption and desorption for further cycles. Figure 12 describes the reusability of CAC/$CoFe_2O_4$200 after a five-cycle number after adsorption–desorption of RhB. The results show that CAC/$CoFe_2O_4$200 could be reused with high RhB removal efficiency of 45.18% after 5^{th} cycle number. It proved that CAC/$CoFe_2O_4$200 is the potential adsorbent for RhB adsorption–desorption from aqueous solution.

4. Conclusions

Through this study, we conclude that activated carbon loaded with $CoFe_2O_4$ composites (CAC/$CoFe_2O_4$200) is a promising type of adsorbent for the riddance of RhB pollutants from aqueous environments. In this study, CAC/$CoFe_2O_4$200 had the ability to adsorb RhB at pH of 4.0. The properties of CAC/$CoFe_2O_4$200 showed that $CoFe_2O_4$ was loaded on the surface of CAC. The results illustrated that the maximum adsorption capacity of CAC/$CoFe_2O_4$200 to RhB was 94.08 mg/g. Freundlich, Langmuir, and pseudo-second-order models appeared highly feasible to describe RhB adsorption onto CAC/$CoFe_2O_4$200. The main adsorption mechanisms of RhB onto CAC/$CoFe_2O_4$200 included the electrostatic attraction, hydrogen bonding interaction, and π-π interaction. Finally, it is possible to conclude that the CAC/$CoFe_2O_4$200 is efficient for adsorbing RhB away from aqueous solutions and should be promoted in the future.

Data Availability

The data used to support the findings of this study are included within the article.

Conflicts of Interest

The authors declare no possible conflicts of interest.

Acknowledgments

The authors would like to acknowledge the financial support from Thai Nguyen University of Technology (TNUT) under grant no. T2019-B27.

References

[1] H. Mittal and S. B. Mishra, "Gum ghatti and Fe_3O_4 magnetic nanoparticles based nanocomposites for the effective adsorption of rhodamine B," *Carbohydrate Polymers*, vol. 101, pp. 1255–1264, 2014.

[2] S. Rahdar, A. Rahdar, M. N. Zafar, S. S. Shafqat, and S. Ahmadi, "Synthesis and characterization of MgO supported Fe-Co-Mn nanoparticles with exceptionally high adsorption capacity for rhodamine B dye," *Journal of Materials Research and Technology*, vol. 8, no. 5, pp. 3800–3810, 2019.

[3] S. K. Das, P. Ghosh, I. Ghosh, and A. K. Guha, "Adsorption of rhodamine B on rhizopus oryzae: role of functional groups and cell wall components," *Colloids and Surfaces B: Biointerfaces*, vol. 65, no. 1, pp. 30–34, 2008.

[4] K. Shen and M. A. Gondal, "Removal of hazardous rhodamine dye from water by adsorption onto exhausted coffee ground," *Journal of Saudi Chemical Society*, vol. 21, pp. S120–S127, 2017.

[5] A. A. Oyekanmi, A. Ahmad, K. Hossain, and M. Rafatullah, "Statistical optimization for adsorption of Rhodamine B dye from aqueous solutions," *Journal of Molecular Liquids*, vol. 281, pp. 48–58, 2019.

[6] L. Azeez, A. Lateef, S. A. Adebisi, and A. O. Oyedeji, *Novel Biosynthesized Silver Nanoparticles from Cobweb as Adsorbent for Rhodamine B: Equilibrium Isotherm, Kinetic and Thermodynamic Studies*, Springer Nature, Basel, Switzerland, 2018.

[7] F. A. Adekola, S. B. Ayodele, and A. A. Inyinbor, "Activated biochar prepared from plaintain peels: characterization and rhodamine B adsorption data set," *Chemical Data Collections*, vol. 19, Article ID 100170, 2019.

[8] J. Anandkumar and B. Mandal, "Adsorption of chromium(VI) and rhodamine B by surface modified tannery waste: kinetic, mechanistic and thermodynamic studies," *Journal of Hazardous Materials*, vol. 186, no. 2-3, pp. 1088–1096, 2011.

[9] J.-H. Huang, K.-L. Huang, S.-Q. Liu, A.-T. Wang, and C. Yan, "Adsorption of rhodamine B and methyl orange on a hypercrosslinked polymeric adsorbent in aqueous solution," *Colloids and Surfaces A: Physicochemical and Engineering Aspects*, vol. 330, no. 1, pp. 55–61, 2008.

[10] H. Lu, Y. Li, Y. Wang, and X. Li, "Preparation of $CoFe_2O_4$@ vacancy@mSiO_2 core-shell composites for removal of organic pollutant in aqueous solution," *Journal of Saudi Chemical Society*, vol. 23, no. 5, pp. 536–545, 2019.

[11] G. Mezohegyi, F. P. van der Zee, J. Font, A. Fortuny, and A. Fabregat, "Towards advanced aqueous dye removal processes: a short review on the versatile role of activated carbon," *Journal of Environmental Management*, vol. 102, pp. 148–164, 2012.

[12] A. R. Bagheri, M. Ghaedi, A. Asfaram, A. A. Bazrafshan, and R. Jannesar, "Comparative study on ultrasonic assisted adsorption of dyes from single system onto Fe_3O_4 magnetite nanoparticles loaded on activated carbon: Experimental design methodology," *Ultrasonics Sonochemistry*, vol. 34, pp. 294–304, 2017.

[13] M. Fayazi, M. Ghanei-Motlagh, and M. A. Taher, "The adsorption of basic dye (Alizarin red S) from aqueous solution onto activated carbon/γ-Fe_2O_3 nano-composite: Kinetic and equilibrium studies," *Materials Science in Semiconductor Processing*, vol. 40, pp. 35–43, 2015.

[14] G. Feiqiang, L. Xiaolei, J. Xiaochen, Z. Xingmin, G. Chenglong, and R. Zhonghao, "Characteristics and toxic dye adsorption of magnetic activated carbon prepared from biomass waste by modified one-step synthesis," *Colloids and Surfaces A: Physicochemical and Engineering Aspects*, vol. 555, pp. 43–54, 2018.

[15] Y. Liang, Y. He, T. Wang, and L. Lei, "Adsorptive removal of gentian violet from aqueous solution using $CoFe_2O_4$/activated carbon magnetic composite," *J. Water Process Eng.*vol. 27, pp. 77–88, July 2018.

[16] L. Ai, H. Huang, Z. Chen, X. Wei, and J. Jiang, "Activated carbon/$CoFe_2O_4$ composites: Facile synthesis, magnetic performance and their potential application for the removal of malachite green from water," *Chemical Engineering Journal*, vol. 156, no. 2, pp. 243–249, 2010.

[17] W. Qiu, D. Yang, J. Xu et al., "Efficient removal of Cr(VI) by magnetically separable $CoFe_2O_4$/activated carbon composite," *Journal of Alloys and Compounds*, vol. 678, pp. 179–184, 2016.

[18] M. Alvarez-Silva, A. Uribe-Salas, M. Mirnezami, and J. A. Finch, "The point of zero charge of phyllosilicate minerals using the mular-roberts titration technique," *Minerals Engineering*, vol. 23, no. 5, pp. 383–389, 2010.

[19] C. R. Ramakrishnaiah and Vismitha, "Removal OF phosphate from wastewater using low-cost adsorbents," *International Journal of Engineering Inventions*, vol. 1, no. 7, pp. 44–50, 2012.

[20] M. Dong, Q. Lin, D. Chen et al., "Amino acid-assisted synthesis of superparamagnetic $CoFe_2O_4$ nanostructures for the selective adsorption of organic dyes," *RSC Advances*, vol. 3, no. 29, pp. 11628–11633, 2013.

[21] M. Zhang, Y. Mao, W. Wang, S. Yang, Z. Song, and X. Zhao, "Coal fly ash/$CoFe_2O_4$ composites: a magnetic adsorbent for the removal of malachite green from aqueous solution," *RSC Advances*, vol. 6, no. 96, pp. 93564–93574, 2016.

[22] J.-H. Park, J. J. Wang, R. Xiao, N. Tafti, R. D. DeLaune, and D.-C. Seo, "Degradation of Orange G by Fenton-like reaction with Fe-impregnated biochar catalyst," *Bioresource Technology*, vol. 249, pp. 368–376, 2018.

[23] N. Yang, S. Zhu, D. Zhang, and S. Xu, "Synthesis and properties of magnetic Fe_3O_4-activated carbon nanocomposite particles for dye removal," *Materials Letters*, vol. 62, no. 4-5, pp. 645–647, 2008.

[24] C. S. Castro, M. C. Guerreiro, M. Gonçalves, L. C. A. Oliveira, and A. S. Anastácio, "Activated carbon/iron oxide composites for the removal of atrazine from aqueous medium," *Journal of Hazardous Materials*, vol. 164, no. 2-3, pp. 609–614, 2009.

[25] L. Ding, B. Zou, W. Gao et al., "Adsorption of rhodamine-B from aqueous solution using treated rice husk-based activated carbon," *Colloids and Surfaces A: Physicochemical and Engineering Aspects*, vol. 446, pp. 1–7, 2014.

[26] R. Jain, M. Mathur, S. Sikarwar, and A. Mittal, "Removal of the hazardous dye rhodamine B through photocatalytic and adsorption treatments," *Journal of Environmental Management*, vol. 85, no. 4, pp. 956–964, 2007.

[27] K. Rachna, A. Agarwal, and N. B. Singh, "pPreparation and characterization of zinc ferrite-polyaniline nanocomposite for removal of rhodamine B dye from aqueous solution," *Environmental Nanotechnology, Monitoring & Management*, vol. 9, pp. 154–163, 2018.

[28] T. A. Khan, S. Dahiya, and I. Ali, "Use of kaolinite as adsorbent: equilibrium, dynamics and thermodynamic studies on the adsorption of rhodamine B from aqueous solution," *Applied Clay Science*, vol. 69, pp. 58–66, 2012.

[29] A. E. Pirbazari, E. Saberikhah, and S. S. H. Kozani, "Fe_3O_4–wheat straw: preparation, characterization and its application for methylene blue adsorption," *Water Resour. Ind.*vol. 7, no. 8, pp. 23–37, 2014.

[30] W. Ding, X. Dong, I. M. Ime, B. Gao, and L. Q. Ma, "Pyrolytic temperatures impact lead sorption mechanisms by bagasse biochars," *Chemosphere*, vol. 105, pp. 68–74, 2014.

[31] I. Langmuir, "The adsorption of gases on plane surfaces of glass, mica and platinum," *Journal of the American Chemical Society*, vol. 40, no. 9, pp. 1361–1403, 1918.

[32] P. Yuan, M. Fan, D. Yang et al., "Montmorillonite-supported magnetite nanoparticles for the removal of hexavalent

chromium [Cr(VI)] from aqueous solutions," *Journal of Hazardous Materials*, vol. 166, pp. 821–829, 2009.

[33] A. A. Inyinbor, F. A. Adekola, and G. A. Olatunji, "Kinetics, isotherms and thermodynamic modeling of liquid phase adsorption of rhodamine B dye onto raphia hookerie fruit epicarp," *Water Resources and Industry*, vol. 15, pp. 14–27, 2016.

[34] J. Zhang, X. Yan, X. Hu, R. Feng, and M. Zhou, "Direct carbonization of Zn/Co zeolitic imidazolate frameworks for efficient adsorption of rhodamine B," *Chemical Engineering Journal*, vol. 347, pp. 640–647, 2018.

[35] G. C. Panda, S. K. Das, and A. K. Guha, "Jute stick powder as a potential biomass for the removal of congo red and rhodamine B from their aqueous solution," *Journal of Hazardous Materials*, vol. 164, no. 1, pp. 374–379, 2009.

[36] D. Wan, W. Li, G. Wang, K. Chen, L. Lu, and Q. Hu, "Adsorption and heterogeneous degradation of rhodamine B on the surface of magnetic bentonite material," *Applied Surface Science*, vol. 349, pp. 988–996, 2015.

[37] S. M. Al-Rashed and A. A. Al-Gaid, "Kinetic and thermodynamic studies on the adsorption behavior of Rhodamine B dye on duolite C-20 resin," *Journal of Saudi Chemical Society*, vol. 16, no. 2, pp. 209–215, 2012.

[38] M. V. Sureshkumar and C. Namasivayam, "Adsorption behavior of direct red 12B and rhodamine B from water onto surfactant-modified coconut coir pith," *Colloids and Surfaces A: Physicochemical and Engineering Aspects*, vol. 317, no. 1-3, pp. 277–283, 2008.

[39] L. Tang, Y. Cai, G. Yang et al., "Cobalt nanoparticles-embedded magnetic ordered mesoporous carbon for highly effective adsorption of rhodamine B," *Applied Surface Science*, vol. 314, pp. 746–753, 2014.

[40] J. Lu, F. Fu, L. Zhang, and B. Tang, "Insight into efficient co-removal of Se (IV) and Cr (VI) by magnetic mesoporous carbon microspheres: performance and mechanism," *Chemical Engineering Journal*, vol. 346, pp. 590–599, 2018.

[41] L. P. Hoang, H. T. Van, L. H. Nguyen et al., "Removal of Cr (vi) from aqueous solution using magnetic modified biochar derived from raw corncob," *New Journal of Chemistry*, vol. 43, no. 47, pp. 18663–18672, 2019.

[42] S. M. Anisuzzaman, C. G. Joseph, Y. H. Taufiq-Yap, D. Krishnaiah, and V. V. Tay, "Modification of commercial activated carbon for the removal of 2, 4-dichlorophenol from simulated wastewater," *Journal of King Saud University - Science*, vol. 27, no. 4, pp. 318–330, 2015.

[43] Y. He, W. Li, G. Yang et al., "A novel method for fabricating wearable, piezoresistive, and pressure sensors based on modified-graphite/polyurethane composite films," *Materials*, vol. 10, no. 7, p. 684, 2017.

[44] A. A. Oyekanmi, A. Ahmad, K. Hossain, and M. Rafatullah, "Adsorption of rhodamine B dye from aqueous solution onto acid treated banana peel: response surface methodology, kinetics and isotherm studies," *PLoS One*, vol. 14, no. 5, pp. 1–20, 2019.

[45] R. Ahmad and R. Kumar, "Adsorption studies of hazardous malachite green onto treated ginger waste," *Journal of Environmental Management*, vol. 91, no. 4, pp. 1032–1038, 2010.

[46] W. Yin, S. Hao, and H. Cao, "Solvothermal synthesis of magnetic $CoFe_2O_4$/rGO nanocomposites for highly efficient dye removal in wastewater," *RSC Advances*, vol. 7, no. 7, pp. 4062–4069, 2017.